

Review

Strategies for Enhancing the Stability of Lithium Metal Anodes in Solid-State Electrolytes

Hanbyeol Lee ¹, Taeho Yoon ^{2,*}  and Oh B. Chae ^{1,*} 

¹ School of Chemical, Biological and Battery Engineering, Gachon University, Seongnam-si 13120, Republic of Korea; byulbbang99@gachon.ac.kr

² Department of Chemical Engineering, Kyung Hee University, Yongin-si 17104, Republic of Korea

* Correspondence: tyoon@khu.ac.kr (T.Y.), obchae@gachon.ac.kr (O.B.C.)

Abstract: The current commercially used anode material, graphite, has a theoretical capacity of only 372 mAh/g, leading to a relatively low energy density. Lithium (Li) metal is a promising candidate as an anode for enhancing energy density; however, challenges related to safety and performance arise due to Li's dendritic growth, which needs to be addressed. Owing to these critical issues in Li metal batteries, all-solid-state lithium-ion batteries (ASSLIBs) have attracted considerable interest due to their superior energy density and enhanced safety features. Among the key components of ASSLIBs, solid-state electrolytes (SSEs) play a vital role in determining their overall performance. Various types of SSEs, including sulfides, oxides, and polymers, have been extensively investigated for Li metal anodes. Sulfide SSEs have demonstrated high ion conductivity; however, dendrite formation and a limited electrochemical window hinder the commercialization of ASSLIBs due to safety concerns. Conversely, oxide SSEs exhibit a wide electrochemical window, but compatibility issues with Li metal lead to interfacial resistance problems. Polymer SSEs have the advantage of flexibility; however their limited ion conductivity poses challenges for commercialization. This review aims to provide an overview of the distinctive characteristics and inherent challenges associated with each SSE type for Li metal anodes while also proposing potential pathways for future enhancements based on prior research findings.

Keywords: Li-ion batteries; Li metal; energy density; solid-state electrolytes



Citation: Lee, H.; Yoon, T.; Chae, O.B. Strategies for Enhancing the Stability of Lithium Metal Anodes in Solid-State Electrolytes. *Micromachines* **2024**, *15*, 453. <https://doi.org/10.3390/mi15040453>

Academic Editors: Bin Liu, Lei Liu and Yaling Wang

Received: 8 March 2024

Revised: 25 March 2024

Accepted: 26 March 2024

Published: 28 March 2024



Copyright: © 2024 by the authors. Licensee MDPI, Basel, Switzerland. This article is an open access article distributed under the terms and conditions of the Creative Commons Attribution (CC BY) license (<https://creativecommons.org/licenses/by/4.0/>).

1. Introduction

Since the commercialization of lithium (Li)-ion batteries (LIBs) in the 1990s, they have been widely applied in various fields, such as small electronic devices, Electric Vehicles (EVs), and Energy Storage Systems (ESSs), owing to their high energy density and stable lifespan [1–4]. Graphite, which is mainly used as the anode material in current LIBs, demonstrates the reversible intercalation/de-intercalation of Li ions between graphene layers, providing stable charge and discharge cycles. However, the theoretical capacity of graphite is limited to approximately 372 mAh/g, posing challenges for high-capacity energy storage [5–8]. Transition metal oxides (e.g., MnO₂, ZnO, Fe₂O₃, and SnO₂) also have gained widespread use as electrode materials in the field of LIBs due to their more substantial theoretical capacities than graphite. Nevertheless, poor cycling performance owing to low electric conductivity and structural collapse as result of large volume expansion during lithiation/delithiation results in poor rate performance and a limited lifespan for LIBs [9]. To overcome this limitation, researchers worldwide are exploring next-generation anode materials for energy storage, including silicon and Li metal.

As Li metal is the lightest member of the alkali metal group and has the lowest reduction voltage (−3.04 V vs. standard hydrogen electrode), extensive research has been reported on highly promising next-generation anode materials [10–12]. However, the use of Li metal in liquid electrolytes faces many challenges owing to its high reactivity to

nonuniform Li dendrite formation, which results in hazardous safety concerns (e.g., fire and explosion). Most of the graphite surface is covered by the reductive decomposition products of electrolyte components created during the initial few cycles. In the case of graphite, owing to the small volume change during the charge and discharge cycle, solid electrolyte interface (SEI) crack generation is mitigated, which minimizes the exposure of the fresh graphite surface during cycling, preventing continuous electrolyte decomposition. On the contrary, the initial SEI of Li metal is generated as soon as the Li metal is exposed to the electrolyte since the electrochemical potential of Li metal is lower than the potential window for the electrolyte components [13–15]. The uncontrolled Li deposition causes the inhomogeneous exposure of fresh Li metal, resulting in low cycling performance and Li dendrite formation.

To overcome the critical issues associated with Li metal, various attempts have been made to suppress Li dendrite growth by using electrolyte additives [16], forming a protective layer [17], and changing the Li salt [18]. However, these approaches present notable challenges in the practical implementation of Li metal batteries. Incorporating solid-state electrolytes (SSEs) into all-solid-state lithium-ion batteries (ASSLIBs) has promise as a method to replace traditional liquid electrolytes. This transition in physical composition suppresses dendrite growth, with SSEs serving dual roles as separators [19,20]. Therefore, when Li metal meets SSEs, the convergence of Li metal with SSEs offers the potential for high energy density and exceptional safety in ASSLIBs.

To realize highly promising ASSLIBs, SSEs should satisfy the following requirements: (1) high ion conductivity at room temperature, (2) a wide electrochemical window, and (3) high chemical compatibility with the Li metal and cathode [21]. They are typically classified into two main categories: inorganic and polymeric forms. Inorganic SSEs can be further categorized into sulfide and oxide types. Understanding the electrochemical characteristics and properties of these three materials is crucial owing to their differences. This review focuses on examining the characteristics and challenges associated with sulfide, oxide, and polymer SSEs when paired with lithium metal, in addition to potential solutions based on previous research.

2. Sulfide SSEs

Sulfide SSEs have demonstrated superior ionic conductivities compared with other solid electrolytes. The high ion conductivity of sulfide SSEs, which is similar to that of organic liquid electrolytes, makes them promising electrolytes for solid-state batteries ($\text{Li}_{10}\text{GeP}_2\text{S}_{12}$, $1.2 \times 10^{-3} \text{ S cm}^{-1}$ [22]; $\text{Li}_2\text{S-P}_2\text{S}_5$, $1.7 \times 10^{-2} \text{ S cm}^{-1}$ [23]). In recent years, Kanno et al. doped the $\text{Li}_{10}\text{GeP}_2\text{S}_{12}$ -type structure LSiPSBrO and obtained $\text{Li}_{9.54}[\text{Si}_{0.6}\text{Ge}_{0.4}]_{1.74}\text{P}_{1.44}\text{S}_{11.1}\text{Br}_{0.3}\text{O}_{0.6}$, the bulk ion conductivity at room temperature of which was determined to be $3.2 \times 10^{-2} \text{ S cm}^{-1}$ [24]. Han et al. demonstrated a different type of sulfide SSE ($\text{Li}_7\text{Si}_2\text{S}_7\text{I}$) created using an ordering of sulfide and iodide [25]. It built a fast transport path of diverse lithium coordination geometries and anion neighbors ($1.01 \times 10^{-2} \text{ S cm}^{-1}$). However, the inherent limitations of sulfide SSEs, such as insufficient dendrite suppression, pose challenges, leading to potential short circuits [26]. Furthermore, their narrow electrochemical window can lead to various reactions with Li metal [27,28], emphasizing the importance of understanding dendrite growth mechanisms and interfacial reactions.

2.1. Challenges of Sulfide SSEs for Li Metal

In liquid electrolytes, Li-ion deposition occurs uniformly owing to consistent contact with Li metal, resulting in an even current density and ion deposition. In contrast, sulfide SSEs exhibit a localized high current density and Li-ion deposition owing to point contact with the Li metal electrode. Consequently, Li dendrite growth and crack formation along crystal boundaries have been reported (Figure 1) [29]. Porz et al. revealed that Li was preferentially deposited on existing cracks or defects, inducing crack-tip stresses and propagation beyond the critical current density [30]. Zhang et al. demonstrated that

alloy materials such as lithium–indium (Li–In) alloys are widely used at the laboratory scale because of their (electro)chemical stability; however, Li–In dendrites grow along the pores and grain boundaries, with high compactness of the $\text{Li}_6\text{PS}_5\text{Cl}$ SSE layer during the charge/discharge process [31].

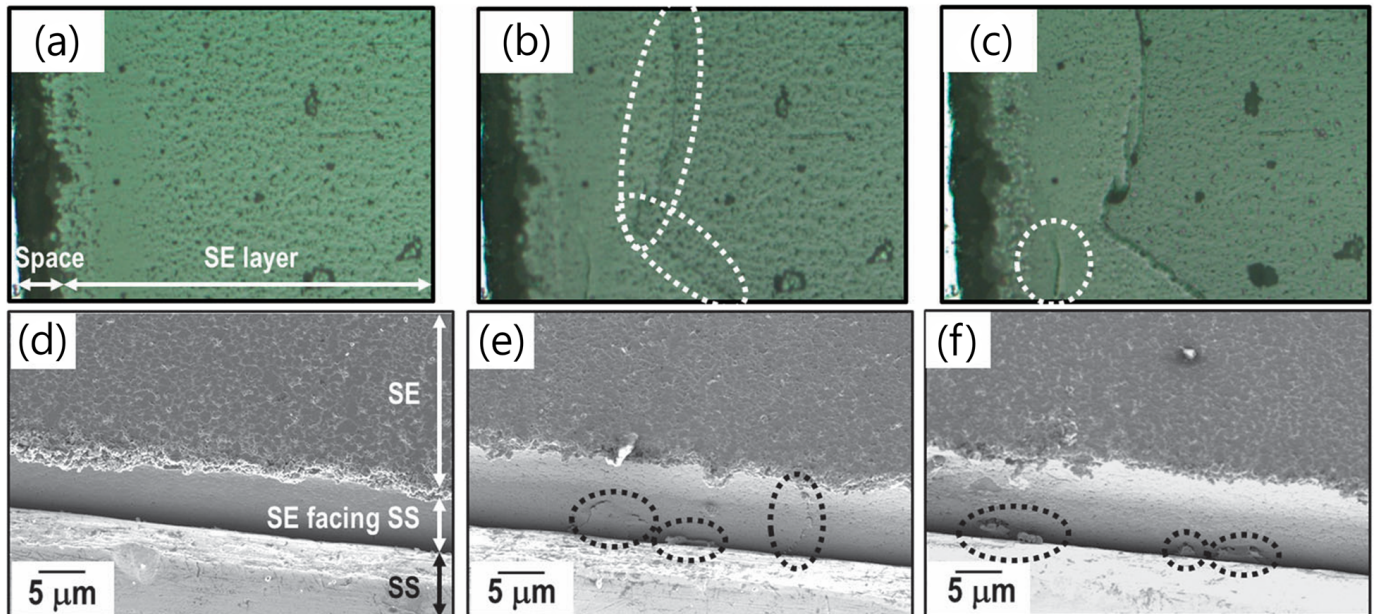


Figure 1. Optical microscope images of the solid electrolyte (SE) layer and the interface between SE and stainless steel (SS): (a) before the test; (b) Li deposition at the interface at 2 mA cm^{-2} for 730 s and (c) at 100 mA cm^{-2} for 2 h. SEM images of the interface between the SE layer and SS at different positions on the same cell (d) before and (e) after Li deposition for 600 s and (f) 1920 s [29]. White arrows showed cracks formed during the charge and discharge process, while black arrows showed inhomogeneous plating of Li. Reprinted with permission from Ref. [29]. Copyright 2013 Royal Society of Chemistry.

In addition, the strong reducing power of Li metal can trigger various reactions at the Li metal–sulfide SSE interface (Figure 2a,b) [27]. In Figure 2a,b, for example, the electrochemical windows of $\text{Li}_{10}\text{GeP}_2\text{S}_{12}$ and Li_3PS_4 are narrow compared to other SSEs. Thus, $\text{Li}_{10}\text{GeP}_2\text{S}_{12}$ and Li_3PS_4 begin to be lithiated and reduced at 1.71 V. Computational studies by Forero et al. using the density functional theory (DFT) and ab initio molecular dynamics (AIMD) demonstrated that sulfide SSE anions (such as PS_4^{3-} , $\text{P}_2\text{S}_6^{2-}$, $\text{P}_2\text{S}_7^{4-}$, and GeS_4^{4-}) react with Li to form Li–S, Li–P, and Li–Ge species (Figure 2c–e) [32]. These studies have demonstrated that sulfide SSEs generate byproducts such as Li_3P , Li_2S , and $\text{Li}_{15}\text{Ge}_4$ during discharge to 0 V, which causes the decomposition of SSEs. Wenzel et al. used XPS to identify compounds formed in sulfide-based SSEs, with $\text{Li}_7\text{P}_3\text{S}_{11}$ exhibiting the lowest resistance among the studied SSEs, resembling the values found in liquid electrolytes [33]. Argyrodite-type sulfide-based SSEs produce SEI layers comprising Li_3P , Li_2S , and decomposed LiX ($X = \text{Cl}$ or Br) [34].

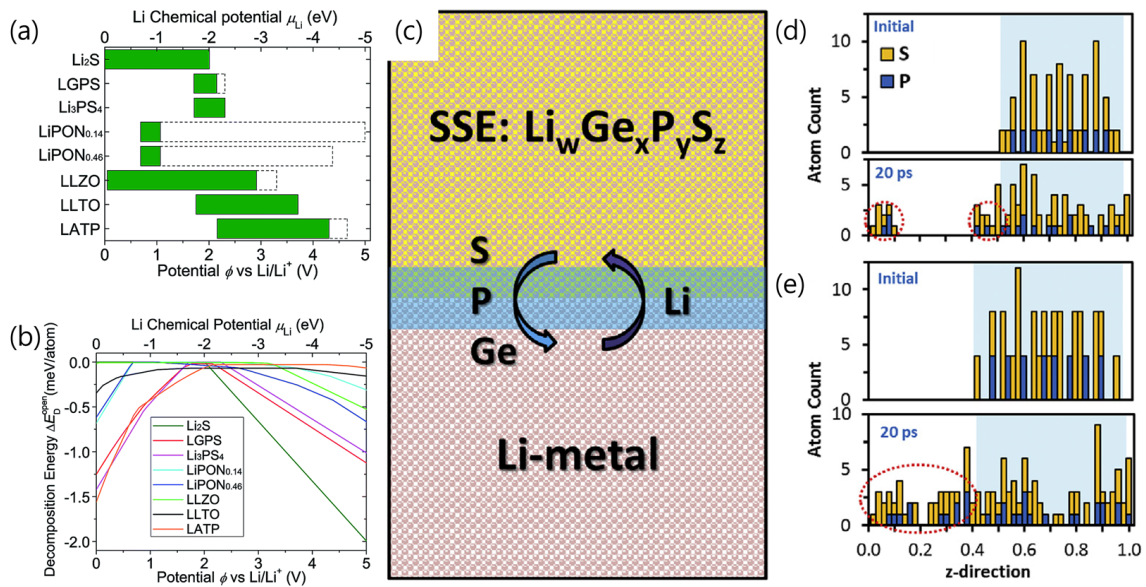


Figure 2. (a) Electrochemical window and (b) decomposition energy [27]. Reprinted with permission from Ref. [27]. Copyright 2013 Royal Society of Chemistry. (c) Schematic representation of interfacial phenomena between sulfide SSEs and Li metal anode. Sulfur and phosphorus atom profiles along z-direction for (d) $\text{Li}_7\text{P}_3\text{S}_{11}$ -(100)/Li-slab and (e) $\text{Li}_2\text{P}_2\text{S}_6$ -(100)/Li slab [32]. At 20 ps, some peaks moved outside the SSE space, which means that some S and P are present at SSE/Li metal interface. Reprinted/adapted with permission from Ref. [32]. Copyright 2018 ELSEVIER.

2.2. Strategies to Overcome Disadvantages of Sulfide SSEs for Li Metal

Wang et al. used a LiF (or LiI) layer at the interface between Li metal and a sulfide SSE and penetrated the sulfide SSE with methoxyperfluorobutane (HFE) (or an I solution) to suppress Li dendrite growth [21]. Li dendrite formation in sulfide SSEs is closely related to the interface stability of the electrolyte with Li metal. The LiF and LiI layers were electrochemically stable in both solid electrolytes and Li metal. The LiF (or LiI) interface layer ensured stability/compatibility at the Li metal/sulfide SSE interface and simultaneously inhibited Li's dendritic growth (Figure 3a,b). Consequently, the interfacial resistance of the cells using LiF- and LiI-coated Li metals was effectively reduced (Figure 3c).

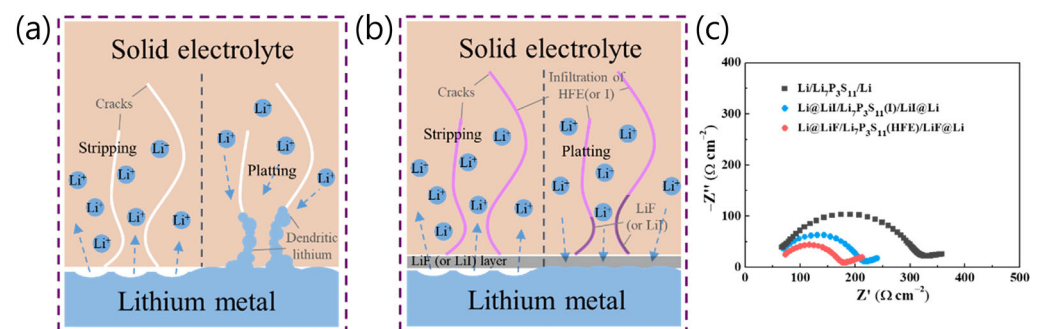


Figure 3. Schematic diagrams of the Li stripping and plating behavior of (a) bare Li metal with an untreated SSE and (b) LiF- or LiI-coated Li metal with HFE- or I-infiltrated electrolyte. (c) Nyquist plots of symmetric cells [21]. Reprinted with permission from Ref. [21]. Copyright 2018 ELSEVIER.

To mitigate dendrite formation and other undesirable reactions, it is crucial to minimize sub-reactions between Li metal and SSEs and SEI formation. The introduction of an artificial SEI has shown promise for inhibiting dendrite growth and ensuring uniform Li deposition. Connell et al. utilized Atomic Layer Deposition (ALD) to create a coating layer on $\text{Li}_6\text{PS}_5\text{Cl}$ sulfide-based SSE powders, resulting in improved stability and a two-fold increase in ion conductivity (Figure 4) [35]. In addition, ALD is a method of depositing thin films which

relies on sequential gas-phase chemical processes. It falls within the broader category of Chemical Vapor Deposition (CVD). The enhanced ion conductivity was attributed to a decrease in the Arrhenius activation energy owing to the coating. Additionally, optimizing the coating thickness is essential to prevent hindered Li^+ conductivity caused by excessively thick Al_2O_3 layers.

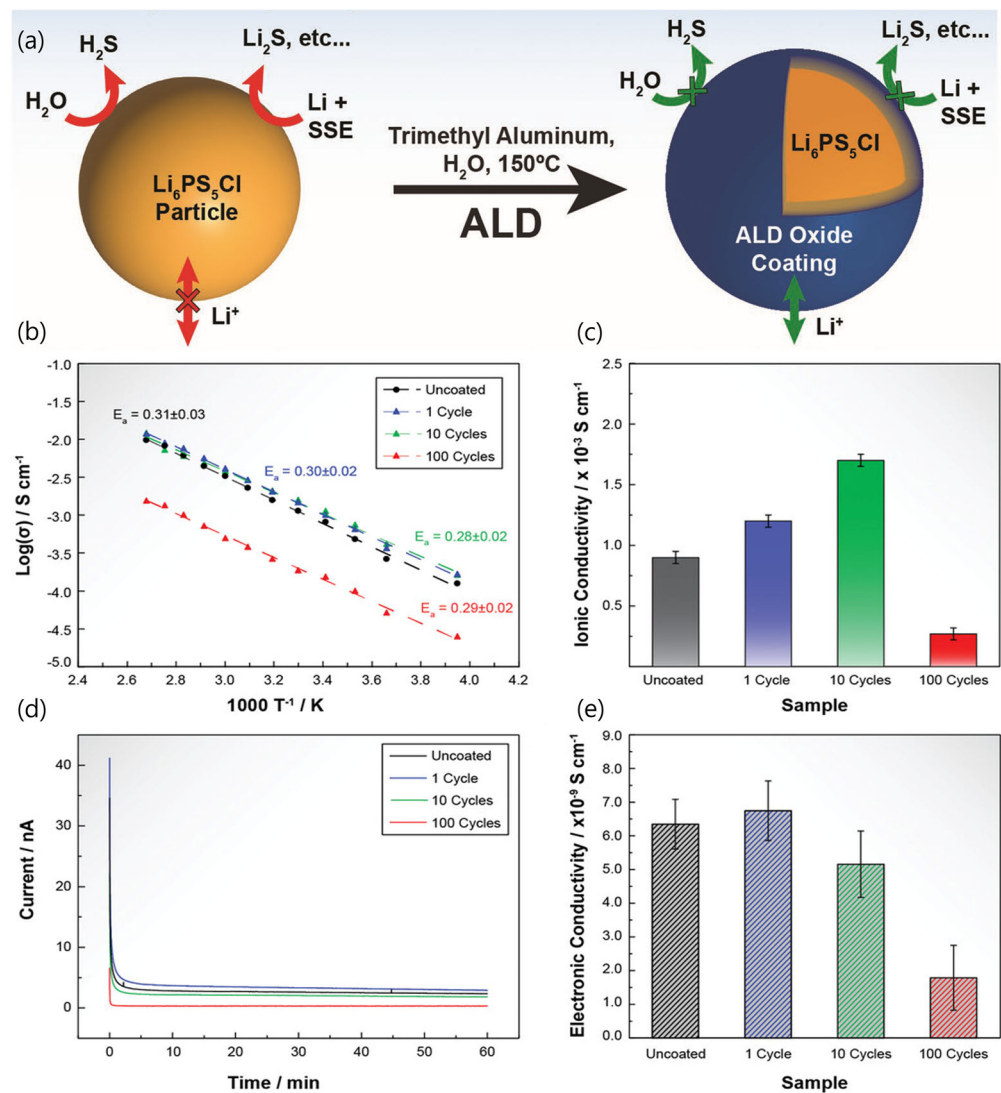


Figure 4. (a) Schematic of the coating strategy based on ALD to produce oxide-coated $\text{Li}_6\text{PS}_5\text{Cl}$ powders. (b) Arrhenius plots, (c) ionic conductivity at 25°C , (d) current versus time (DC polarization at 200 mV ; 25°C), and (e) electronic conductivity at 25°C for $\text{Li}_6\text{PS}_5\text{Cl}$ pellets pressed from powders coated by 1, 10, and 100 ALD alumina cycles in comparison to pellets pressed from uncoated powders [35]. Reprinted with permission from Ref. [35]. Copyright 2023 Wiley-VCH.

Furthermore, altering the composition of sulfide SSEs is an effective strategy. Composition tuning has proven to be effective in enhancing stability and controlling decomposition products, thereby preventing material propagation and reducing interfacial resistance. Sulfide SSE tuning is categorized into cation substitution and anion substitution, depending on the atoms comprising the structure. In a previous study, research was conducted to improve the performance of sulfide SSEs through cation substitution. Substituting a cation (e.g., Ge with Si, Sn, Al, P, Ba, Zn, or Y in LGPS) can adjust the stability of sulfide SSEs with minimal impact on material properties such as ion conductivity, as indicated by first-principles calculations [36]. However, this study demonstrates that Si, Sn, and Ge are also unstable versus Li and tend to form non-passivating degradation products on the Li metal. Research

has also been conducted on anion substitution in addition to cation substitution. The partial substitution of an anion, especially sulfur by oxygen, has been shown to increase the thermodynamic stability of $\text{Li}_{10}\text{GeP}_2\text{S}_{12}$ by providing stronger chemical bonding, and oxygen substitution was recently used to stabilize the $\text{Li}_{10}\text{GeP}_2\text{S}_{12}$ -phase of Li_3PS_4 [37,38].

3. Oxide SSEs

Oxide SSEs exhibit substantial energy gaps between their valence and conduction bands which provide enhanced stability at elevated voltages. In addition, the ionic mobility of oxide SSEs surpasses that of polymer electrolytes. Among the various oxide SSEs, garnet-type SSEs have the highest ion conductivity. The garnet-type $\text{Li}_7\text{La}_3\text{Zr}_2\text{O}_{12}$ (LLZO) oxide SSE synthesized by Weppner et al. is particularly attractive because of its good stability against Li metal, large electrochemical window, and easy handling in ambient environments [39–41]. The LLZO SSEs exhibit the best resistance to Li reduction and have the lowest reduction potential (approximately 0.05 V vs. Li/Li^+) and the most stable interface.

3.1. Challenges of Oxide SSEs for Li Metal

Several studies have shown that the absorbed CO_2 reacts directly with Li in the garnet structure to form Li_2CO_3 (Equation (1)) [42]. The Li_2CO_3 on the surface of the Li metal increases the interfacial resistance and decreases the ion conductivity (Figure 5) [43]. Cheng et al. reported that the large impedance at the LLZO/Li metal interface is not inherent to the material; however, it originates from the Li_2CO_3 due to ambient air exposure [44].

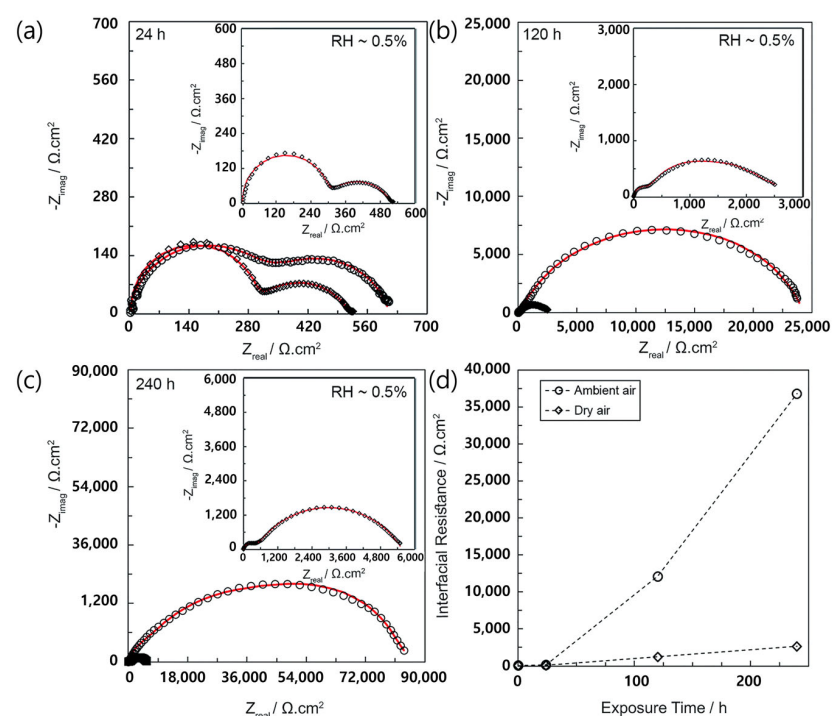
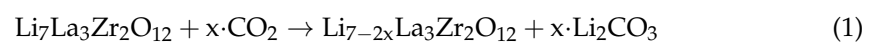


Figure 5. Impedance spectra measured at room temperature for Li metal symmetric cells after various exposure times to ambient (\circ) and dry air (\diamond). Schematic depicting the asymmetric Li metal symmetric cell before and after air exposure and equivalent circuit model used for fitting EIS data at (a) 24 h, (b) 120 h, and (c) 240 h. The insets display the impedance spectra for Li-LLZO-Li for samples exposed to dry air. (d) The LLZO/Li metal interfacial resistance versus time after exposure to ambient and dry air [43]. Reprinted with permission from Ref. [43]. Copyright 2017 Royal Society of Chemistry.

Another interface problem is the low wettability between garnet-type oxide SSEs and Li metal. When LLZO SSEs were manufactured through compression at room temperature, the particles did not agglomerate, and void spaces were present within the resulting structures (Figure 6) [45]. The rigid connection between the electrode and the SSEs and the existence of an inert surface layer of Li_2CO_3 resulted in poor interface compatibility, which led to an interfacial impedance of $10^2\sim 10^3 \Omega \text{ cm}^2$ and thus unstable Li plating and stripping [46,47].

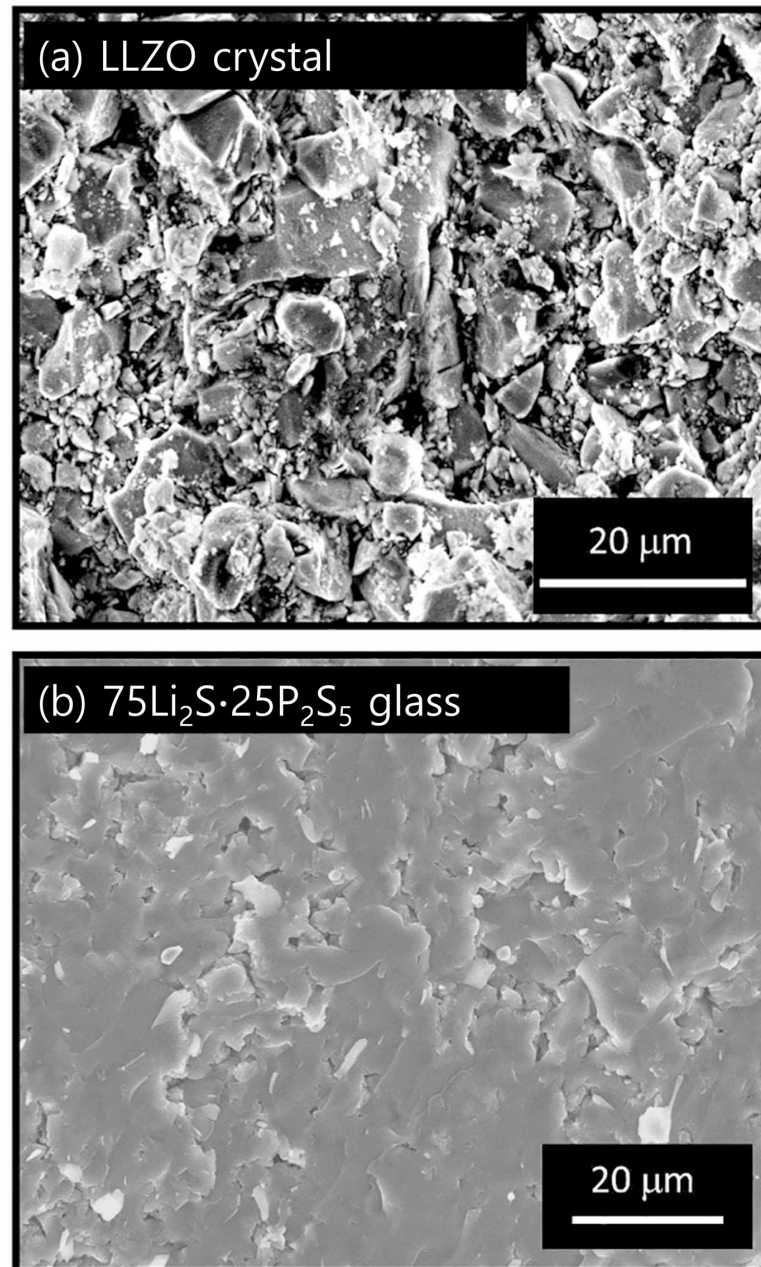


Figure 6. Fracture cross-section SEM images of (a) LLZO and (b) sulfide electrolyte particles glass-pelletized at room temperature [45]. Reprinted with permission from Ref. [45]. Copyright 2013 Nature Publishing Group.

3.2. Strategies to Overcome Disadvantages of Oxide SSEs for Li Metal

Many studies have reported methods to eliminate Li_2CO_3 , a factor that increases interfacial resistance (e.g., by carbothermal reactions, high-temperature calcination, or acid treatment) [48–50]. Furthermore, both dry and wet polishing have been reported to be

effective approaches for removing Li_2CO_3 from a surface [13,51]. Sakamoto et al. noted that among the two approaches, dry and wet polishing, the latter was mentioned as the more effective method for removing Li_2CO_3 (Figure 7a–d) [51].

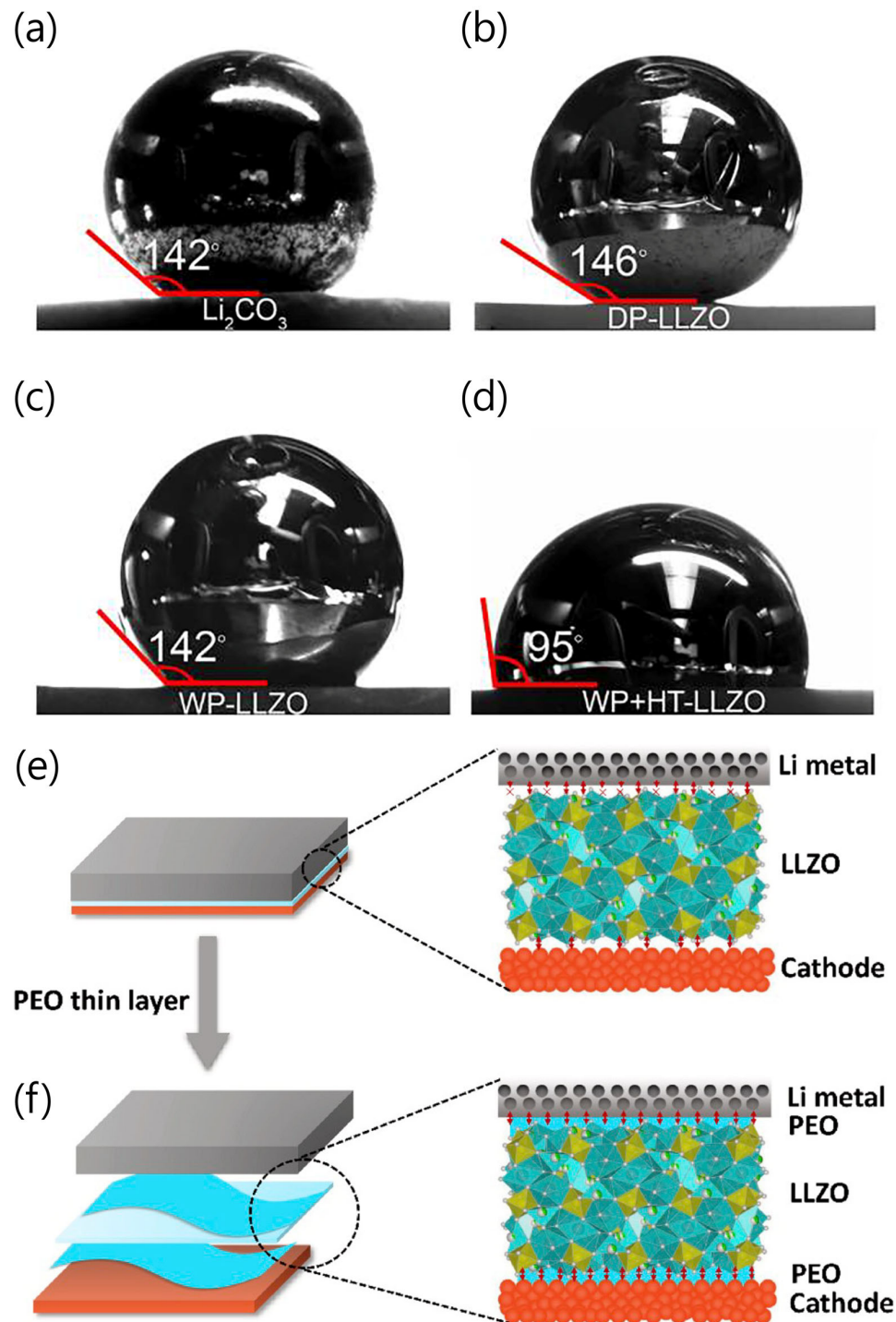


Figure 7. Contact angle measurements of molten metallic on (a) Li_2CO_3 , (b) dry polishing of LLZO, (c) wet polishing of LLZO, and (d) wet polishing of LLZO after heat treatment at 500°C [51]. Reprinted with permission from Ref. [51]. Copyright 2017 American Chemical Society. Schematic of electrode–LLZO interface for solid-state battery. (e) Hard-to-hard interfaces with bad contact between electrodes and LLZO. (f) Soft-to-hard interfaces with improved connection [52]. Reprinted with permission from Ref. [52]. Copyright 2020 ELSEVIER.

A common strategy for overcoming point contacts with Li metal is to use an artificial interface layer. The excellent flexibility and softness of polymers can enhance the low interface contact between LLZO and Li metal. Flexible polymers can serve as coatings for LLZO and electrodes, resembling the characteristics found in liquid electrolytes, and are advantageous for scalable processing. Yang et al. developed a thin polyethylene oxide (PEO) buffer layer to modify LLZO (Figure 7e,f) [52]. In their study, the interfacial resistance decreased from $1360 \Omega \text{ cm}^2$ to $175 \Omega \text{ cm}^2$ and exhibited good stability to Li metal at 0.2 mA cm^{-2} . PEO-Poly(acrylamide-2-methyl-1-propane-sulfonate) (PAS)-coated $\text{Li}_{6.5}\text{La}_3\text{Zr}_{1.5}\text{Ta}_{0.5}\text{O}_{12}$ (LLZTO) was demonstrated by Zhou et al. [53]. PAS is a Li^+ -conducting polymer which carries out the transportation of high amounts of Li^+ . The interfacial impedance of Li/LLZTO/Li was around 5000Ω , while a Li/PEO-PAS/LLZTO/PEO-PAS/Li cell exhibited an interfacial impedance of less than 400Ω . Owing to good Li ion transport and contact with Li metal, the capacity retention was around 137 mAh/g at 0.2 C after 160 cycles.

In addition, Goodenough et al. designed a cell utilizing a cross-linked polymer, poly(ethylene glycol) methyl ether acrylate (CPMEA), as a buffer layer between the cathode and Li metal (Figure 8a,b) [54]. The polymer layer not only improved contact at the interface because of its flexibility and softness but also increased the Li^+ flux, thereby improving the cycling performance and preventing dendrite formation in the cell.

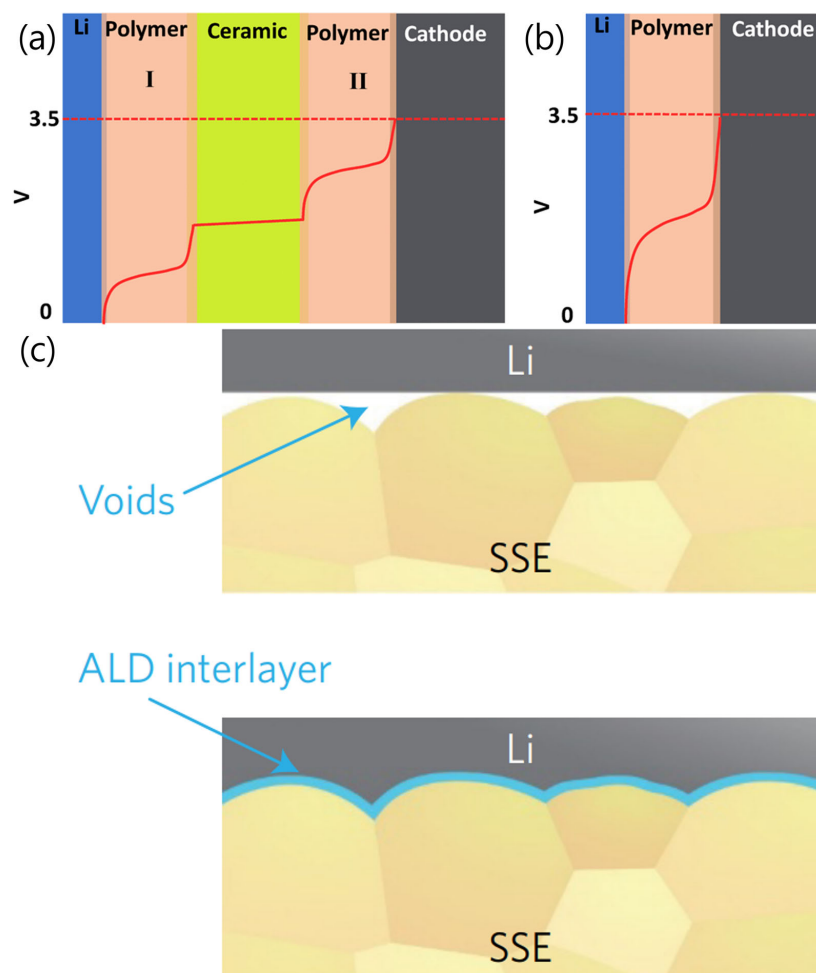


Figure 8. Schematic of the electric potential profile across the (a) sandwich electrolyte and (b) individual polymer electrolyte in the charge process of a full cell [54]. Both polymer I and II represent CPMEA. Reprinted with permission from Ref. [54]. Copyright 2016 American Chemical Society. (c) Schematic of the behavior of LLZO with molten Li metal [55]. Reprinted with permission from Ref. [55]. Copyright 2017 Nature Publishing Group.

Similar to the approach described for sulfide SSEs, there is a method employing ALD to form a thin film at the Li metal and LLZO interface, effectively improving wettability and reducing resistance. Hu et al. demonstrated that the wettability of SSEs against molten Li was significantly improved by applying an alumina ALD coating [55]. The LLZO/Li metal interfacial resistance decreased from $1710 \Omega \text{ cm}^2$ to $34 \Omega \text{ cm}^2$ owing to Li metal on a lithiated pure alumina layer with a varied Li stoichiometry, $\text{Li}_x\text{Al}_2\text{O}_{3+x/2}$; a strong chemical bond with the Li metal formed, and it exhibited good ion conductivity (Figure 8c). Various metals and metal oxides, including Si, ZnO, and Au, have been reported in studies in which ALD was employed for coating. These materials demonstrated enhanced wettability with molten Li and concurrently reduced interfacial resistance [56–58].

4. Polymer SSEs

Polymer SSEs are predominantly composed of thermally stable polymers, such as the previously mentioned polymers PEO, poly(vinylidene fluoride) (PVDF), and polyacrylonitrile (PAN). Among these, PEO, which can form various salts through interactions between ether oxygen atoms and cations, has been extensively studied as a dry polymer electrolyte host. Its ability to dissolve various salts makes it the most widely studied dry polymer electrolyte host. Consequently, they can be utilized in the design of all-solid-state batteries with self-supporting films without altering current battery assembly processes [59]. In addition, gel-formulated polymer electrolytes have been reported as various types of polymer solid-state electrolytes. In this configuration, the liquid components within the gel facilitate ion conduction. In this review, no detailed exposition is provided on this subject.

4.1. Challenges of Polymer SSEs for Li Metal

PEO-based electrolytes generally exhibit low ion conductivity at an order of 10^{-8} – $10^{-7} \text{ S cm}^{-1}$ at room temperature because the ion conduction in the PEO-based electrolyte mainly occurs in the amorphous part of the PEO matrix, while the crystalline part provides very limited ion motion (note that the PEO chain is mainly crystalline below 65°C) [60,61]. The Li^+ ion conduction mechanisms of both the amorphous and crystalline polymers are shown in Figure 9 [62].

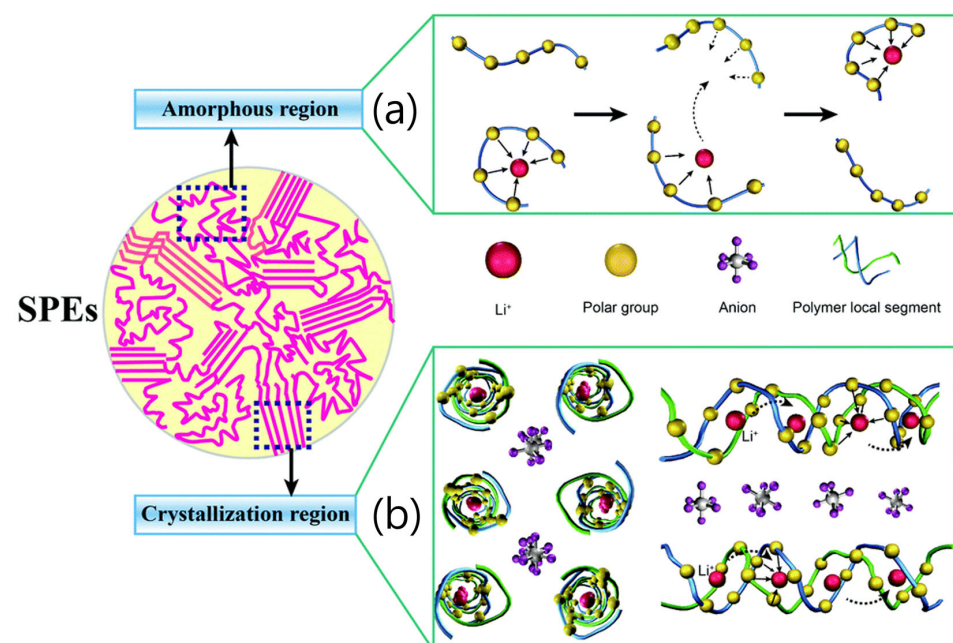


Figure 9. Schematic of conduction mechanism in two kinds of polymer electrolytes. (a) Amorphous polymer electrolytes and (b) crystalline polymer electrolytes [62]. Reprinted with permission from Ref. [62]. Copyright 2016 Royal Society of Chemistry.

Moreover, most polymer electrolytes are dual-ion conductors in which Li^+ and its counter anions are both mobile. Therefore, Li^+ is coupled with Lewis basic sites in the polymer matrix; thus, Li^+ is usually less mobile than anions. Therefore, the Li^+ transference number of ion conductors with dual ions is generally lower than 0.5. Li^+ ; in addition, counter anions move in opposite directions during discharge cycles, leading to the accumulation of anions at the anode side and causing concentration gradients and cell polarization (Figure 10) [63,64]. The transference number is defined as the ratio of the electric current derived from the cation to the total electric current. If the number is close to one, it implies that the ion-conducting performance of the polymer electrolyte is mainly accomplished by the cation [65].

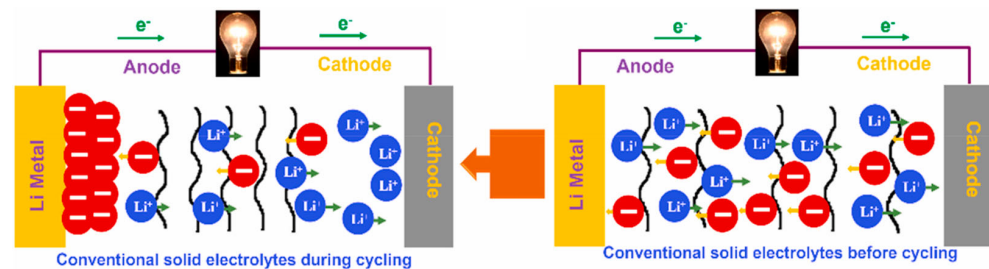


Figure 10. The operational phenomena of conventional SPEs [64]. Reprinted with permission from Ref. [64]. Copyright 2021 ELSEVIER.

4.2. Strategies to Overcome Disadvantages of Polymer SSEs for Li Metal

Among the various methods available, polymer blending is the most feasible. Polymer blending involves mixing at least two polymers, with or without chemical bonding [66]. Poly(methyl methacrylate) (PMMA)- and PVDF-blended polymer electrolytes were demonstrated by Nicotera et al. [67]. Oscillatory rheological tests showed better mechanical properties for the intermediate composition of the blend (Figure 11a,b). Subsequently, Ganessan et al. [49] studied the design of blended polymer electrolytes using machine learning [68]. Electrolyte performance was measured using a combination of ionic transport and electrolyte mechanical properties. In this study, through the utilization of a machine learning approach known as Bayesian optimization, a trade-off between ion transport and electrolyte mechanical properties was identified as a function of various design parameters, including host molecular weight and polarity.

Copolymer electrolytes may be considered a method for reducing crystalline PEO. A copolymer is a polymer composed of multiple monomer species. Copolymer electrolytes exhibit conductivities exceeding $10^{-4} \text{ S cm}^{-1}$ at room temperature which result from the highly amorphous structure of the studied polymer hosts and their high flexibility, as evidenced by a T_g value below 210 K [69]. Recently, Li et al. reported the synthesis of copolymers through cationic ring-opening polymerization using 1,3-dioxolane (DOL) and trioxymethylene (TOM) as monomers [70]. The ion conductivity from the study by Li et al. reached $3.56 \times 10^{-4} \text{ S cm}^{-1}$ at room temperature (Figure 11c).

The use of single-ion conducting polymer electrolytes (SICPEs), ideally defined as polymer electrolytes with Li^+ transference numbers similar to unity (approximately 1), can be an effective method for reducing concentration polarization. With a higher transference number than traditional polymer electrolytes, SICPEs exhibit remarkably decreased polarization, which should theoretically allow them to suppress Li dendrites [71–74]. Conventional SICPEs are fabricated by covalently bonding anions to the polymer backbone, allowing only single-ion species to be mobile. Gohy et al. reported a copolymer electrolyte combining a single-ion conducting anionic group (poly(lithium methacrylate-co-oligoethylene glycol methacrylate)) [75]. Its ion conductivity reached up to $2 \times 10^{-5} \text{ S cm}^{-1}$. Mecerreyes et al. developed SICPEs based on UV-cross-linkable polyurethanes [76]. A coulombic efficiency near 100% and capacity retention exceeding 72.8% were measured after 80 cycles at 0.1 C. The ion conductivities and properties of the other SICPEs are displayed in Figure 12 and Table 1 [77].

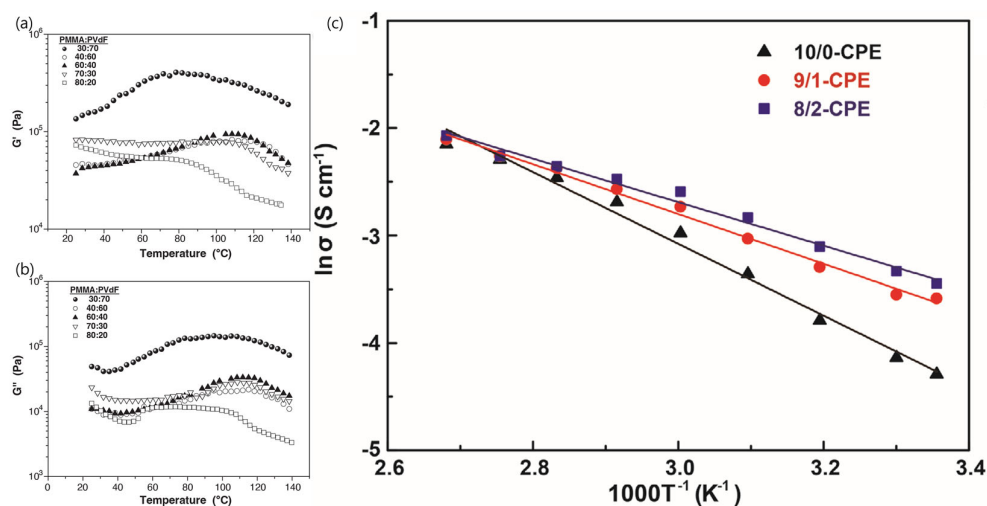


Figure 11. Temperature sweep test from 25 to 140 °C of (a) G' vs. temperature and (b) G'' vs. temperature [67]. Reprinted with permission from Ref. [67]. Copyright 2006 ELSEVIER. (c) The ion conductivity of DOL and TOM copolymer electrolytes in a temperature range of 25–110 °C (black, red, and blue lines represent the DOL/TOM molar ratio as 10/0, 9/1, and 8/2, respectively) [70]. Reprinted with permission from Ref. [70]. Copyright 2020 Wiley-VCH.

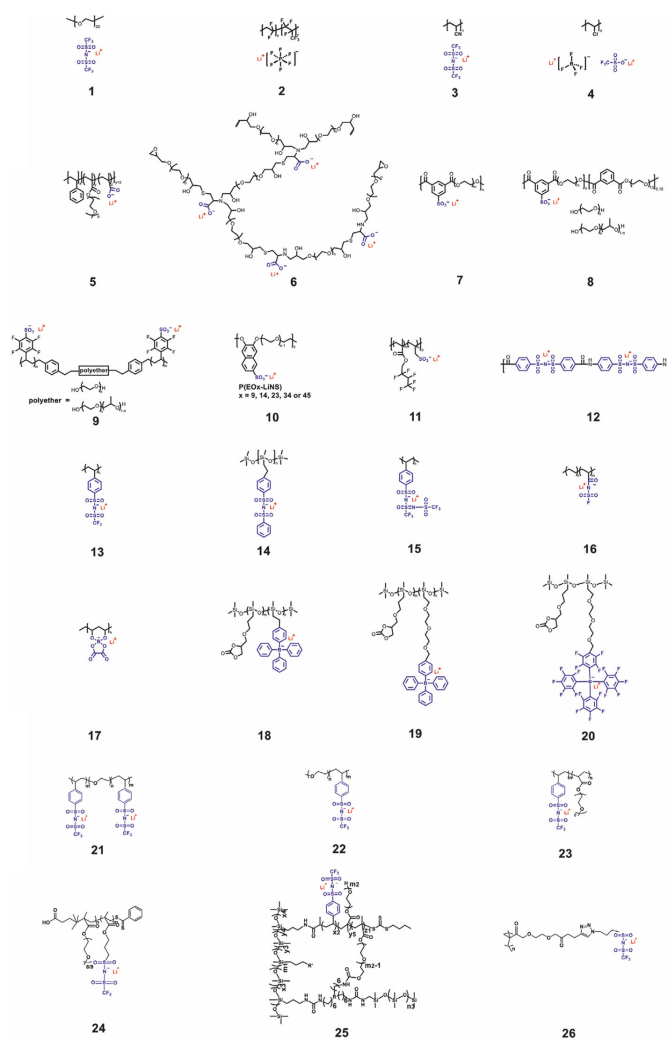


Figure 12. Representative structures of the reported SICPEs [77]. Reprinted with permission from Ref. [77]. Copyright 2021 Wiley-VCH.

Table 1. Summary of various SICPEs with corresponding property parameters [77]. Reused with permission from Ref. [77]. Copyright 2021 Wiley-VCH.

Materials	T _g [°C]	t _{Li⁺}	Ionic Conductivity [S cm ⁻¹]	Testing Temperature [°C]	Mechanical Strength [MPa]
1	-57	0.29	N/A	N/A	N/A
2	N/A	0.46	8.9×10^{-4}	25	N/A
3	-105.2	N/A	2.5×10^{-3}	23	N/A
4	N/A	N/A	2.6×10^{-3}	25	N/A
5	N/A	Close to unity	$\approx 10^{-8}$	20	N/A
6	<0	0.86	1.2×10^{-4}	85	N/A
7	-37	N/A	10^{-6}	25	N/A
8	-20	N/A	$\approx 10^{-5}$	25	N/A
9	<0	N/A	1.4×10^{-5}	60	N/A
10	-38	N/A	5.5×10^{-6}	120	N/A
11	17	0.92	10^{-4}	80	7.1
12	N/A	0.92	1.4×10^{-4}	25	N/A
13	152	N/A	$\approx 10^{-5}$	41	N/A
14	-110	0.89	7.2×10^{-4}	25	5.8
15	-47	>0.9	7.6×10^{-6}	25	N/A
16	-30	0.91	5.84×10^{-4}	25	N/A
17	N/A	N/A	6.11×10^{-6}	25	N/A
18	10	N/A	$10^{-8.2}$	25	N/A
19	-17	N/A	$10^{-7.0}$	25	N/A
20	-16	N/A	$10^{-6.9}$	25	N/A
21	N/A	0.85	1.35×10^{-5}	60	10
22	N/A	0.95	3.8×10^{-4}	90	N/A
23	<0	>0.9	10^{-4}	60	N/A
24	-61	0.83	2.3×10^{-6}	25	N/A
25	-17.5	0.79	4.5×10^{-7}	30	0.37
26	-27 to -14	0.79–0.99	10^{-5} – 10^{-4}	90	N/A

5. Conclusions

In this review, the properties, challenges, and previous studies of sulfide, oxide, and polymer SSEs for Li metal anodes were examined. Despite the high theoretical capacity and energy density of lithium metal, its commercialization is challenging when using liquid electrolytes. This challenge has led to extensive research on SSEs. Due to the varying physical and chemical properties of each SSE, the challenges and improvement strategies for Li metal anodes also differ. At the interfaces between sulfide SSEs and lithium metal, challenges such as lithium dendrite formation and side reactions are prevalent. Various methods can be employed to tackle these issues, including applying interlayers, utilizing ALD coatings, and optimizing the electrolyte composition. In the case of oxide SSEs, significant hurdles arise from substantial interfacial resistance due to point contact with lithium metal and impurity generation from reactions with CO₂. These challenges can be alleviated through techniques such as polishing, employing buffer layers, and implementing ALD coatings similar to those used for sulfide SSEs. Polymer SSEs encounter challenges associated with low ionic conductivity and concentration polarization, which can potentially lead to lithium dendrite formation. Addressing these issues involves strategies like polymer blending, copolymerization, and the utilization of solid ion-conducting polymer electrolytes. Despite these efforts, numerous technical and commercial challenges remain in the commercialization of solid-state electrolytes (SSEs). However, with a thorough understanding of SSEs and ongoing research on Li metal anodes and cathodes, the commercialization of ASSLIBs is expected to be achieved.

Funding: This work was supported by the Gachon University Research Fund of 2022 (GCU-202301000001).

Conflicts of Interest: The authors declare no conflicts of interest.

References

1. Yoon, D.H.; Park, Y.J. Electrochemical Properties of Cathode According to the Type of Sulfide Electrolyte and the Application of Surface Coating. *J. Electrochem. Sci. Technol.* **2021**, *12*, 126–136. [[CrossRef](#)]
2. Zhao, W.; Choi, W.; Yoon, W.-S. Nanostructured electrode materials for rechargeable lithium-ion batteries. *J. Electrochem. Sci. Technol.* **2020**, *11*, 195–219. [[CrossRef](#)]
3. Adiraju, V.A.K.; Chae, O.B.; Robinson, J.R.; Lucht, B.L. Highly Soluble Lithium Nitrate-Containing Additive for Carbonate-Based Electrolyte in Lithium Metal Batteries. *ACS Energy Lett.* **2023**, *8*, 2440–2446. [[CrossRef](#)]
4. Kwon, K.; Kim, J.; Han, S.; Lee, J.; Lee, H.; Kwon, J.; Lee, J.; Seo, J.; Kim, P.J.; Song, T. Low-Resistance LiFePO₄ Thick Film Electrode Processed with Dry Electrode Technology for High-Energy-Density Lithium-Ion Batteries. *Small Sci.* **2024**, 2300302. [[CrossRef](#)]
5. Lee, G.; Kim, I.T.; Hur, J. Highly conductive and robust telluride-carbon hybrid matrix for enhanced copper diphosphide anode in Li-ion batteries. *J. Alloys Compd.* **2023**, *950*, 169914. [[CrossRef](#)]
6. Thieu, Q.Q.V.; Kidanu, W.G.; Nguyen, H.D.; Nguyen, T.L.T.; Le, M.L.P.; Nguyen, D.Q.; Tran, N.T.; Nguyen, X.V.; Kim, I.T.; Nguyen, T.L. Spinel Ni-ferri advanced high-capacity anode for Li-ion batteries prepared via coprecipitation route. *Ceram. Int.* **2022**, *48*, 31470–31477. [[CrossRef](#)]
7. Nguyen, Q.H.; Kim, I.T.; Hur, J. Core-shell Si@c-PAN particles deposited on graphite as promising anode for lithium-ion batteries. *Electrochim. Acta* **2019**, *297*, 355–364. [[CrossRef](#)]
8. Lim, Y.E.; Choi, W.S.; Kim, J.H.; Ahn, Y.N.; Kim, I.T. The Sn–red P–Fe–based alloy materials for efficient Li–ion battery anodes. *J. Ind. Eng. Chem.* **2023**, *121*, 299–311. [[CrossRef](#)]
9. Tran, Q.N.; Park, C.H.; Le, T.H. Nanocrystalline Cellulose-Supported Iron Oxide Composite Materials for High-Performance Lithium-Ion Batteries. *Polymers* **2024**, *16*, 691. [[CrossRef](#)]
10. Cheng, X.B.; Zhang, R.; Zhao, C.Z.; Zhang, Q. Toward Safe Lithium Metal Anode in Rechargeable Batteries: A Review. *Chem. Rev.* **2017**, *117*, 10403–10473. [[CrossRef](#)]
11. Yang, S.; Kim, J.; Lee, S.; Seo, J.; Choi, J.; Kim, P.J. Uniform Li Deposition through the Graphene-Based Ion-Flux Regulator for High-Rate Li Metal Batteries. *ACS Appl. Mater. Interfaces* **2024**, *16*, 3416–3426. [[CrossRef](#)]
12. Paul, S. Materials and electrochemistry: Present and future battery. *J. Electrochem. Sci. Technol.* **2016**, *7*, 115–131. [[CrossRef](#)]
13. Chae, O.B.; Lucht, B.L. Interfacial Issues and Modification of Solid Electrolyte Interphase for Li Metal Anode in Liquid and Solid Electrolytes. *Adv. Energy Mater.* **2023**, *13*, 2203791. [[CrossRef](#)]
14. Chae, O.B.; Kim, J.; Lucht, B.L. Modification of lithium electrodeposition behavior by variation of electrode distance. *J. Power Sources* **2022**, *532*, 231338. [[CrossRef](#)]
15. Kim, M.; Park, H.G.; Park, K. A strategy of enhancing the ionic conductivity of Li₇La₃Zr₂O₁₂ under accurate sintering conditions. *Phys. Chem. Chem. Phys.* **2022**, *24*, 29159–29164. [[CrossRef](#)] [[PubMed](#)]
16. Zhang, X.-Q.; Cheng, X.-B.; Chen, X.; Yan, C.; Zhang, Q. Fluoroethylene Carbonate Additives to Render Uniform Li Deposits in Lithium Metal Batteries. *Adv. Funct. Mater.* **2017**, *27*, 1605989. [[CrossRef](#)]
17. Fan, L.; Zhuang, H.L.; Gao, L.; Lu, Y.; Archer, L.A. Regulating Li deposition at artificial solid electrolyte interphases. *J. Mater. Chem. A* **2017**, *5*, 3483–3492. [[CrossRef](#)]
18. Jurng, S.; Brown, Z.L.; Kim, J.; Lucht, B.L. Effect of electrolyte on the nanostructure of the solid electrolyte interphase (SEI) and performance of lithium metal anodes. *Energy Environ. Sci.* **2018**, *11*, 2600–2608. [[CrossRef](#)]
19. Sun, C.; Liu, J.; Gong, Y.; Wilkinson, D.P.; Zhang, J. Recent advances in all-solid-state rechargeable lithium batteries. *Nano Energy* **2017**, *33*, 363–386. [[CrossRef](#)]
20. Gao, Z.; Sun, H.; Fu, L.; Ye, F.; Zhang, Y.; Luo, W.; Huang, Y. Promises, challenges, and recent progress of inorganic solid-state electrolytes for all-solid-state lithium batteries. *Adv. Mater.* **2018**, *30*, 1705702. [[CrossRef](#)]
21. Xu, R.; Han, F.; Ji, X.; Fan, X.; Tu, J.; Wang, C. Interface engineering of sulfide electrolytes for all-solid-state lithium batteries. *Nano Energy* **2018**, *53*, 958–966. [[CrossRef](#)]
22. Kamaya, N.; Homma, K.; Yamakawa, Y.; Hirayama, M.; Kanno, R.; Yonemura, M.; Kamiyama, T.; Kato, Y.; Hama, S.; Kawamoto, K. A lithium superionic conductor. *Nat. Mater.* **2011**, *10*, 682–686. [[CrossRef](#)] [[PubMed](#)]
23. Seino, Y.; Ota, T.; Takada, K.; Hayashi, A.; Tatsumisago, M. A sulphide lithium super ion conductor is superior to liquid ion conductors for use in rechargeable batteries. *Energy Environ. Sci.* **2014**, *7*, 627–631. [[CrossRef](#)]
24. Li, Y.; Song, S.; Kim, H.; Nomoto, K.; Kim, H.; Sun, X.; Hori, S.; Suzuki, K.; Matsui, N.; Hirayama, M. A lithium superionic conductor for millimeter-thick battery electrode. *Science* **2023**, *381*, 50–53. [[CrossRef](#)] [[PubMed](#)]
25. Han, G.; Vasylenko, A.; Daniels, L.M.; Collins, C.M.; Corti, L.; Chen, R.; Niu, H.; Manning, T.D.; Antypov, D.; Dyer, M.S. Superionic lithium transport via multiple coordination environments defined by two-anion packing. *Science* **2024**, *383*, 739–745. [[CrossRef](#)] [[PubMed](#)]
26. Chen, S.; Xie, D.; Liu, G.; Mwiszerwa, J.P.; Zhang, Q.; Zhao, Y.; Xu, X.; Yao, X. Sulfide solid electrolytes for all-solid-state lithium batteries: Structure, conductivity, stability and application. *Energy Storage Mater.* **2018**, *14*, 58–74. [[CrossRef](#)]

27. Zhu, Y.; He, X.; Mo, Y. First principles study on electrochemical and chemical stability of solid electrolyte–electrode interfaces in all-solid-state Li-ion batteries. *J. Mater. Chem. A* **2016**, *4*, 3253–3266. [[CrossRef](#)]
28. Lee, J.Y.; Park, Y.J. Li₃PO₄ Coated Li[Ni_{0.75}Co_{0.1}Mn_{0.15}]O₂ Cathode for All-Solid-State Batteries Based on Sulfide Electrolyte. *J. Electrochem. Sci. Technol.* **2022**, *13*, 407–415. [[CrossRef](#)]
29. Nagao, M.; Hayashi, A.; Tatsumisago, M.; Kanetsuku, T.; Tsuda, T.; Kuwabata, S. In situ SEM study of a lithium deposition and dissolution mechanism in a bulk-type solid-state cell with a Li₂S–P₂S₅ solid electrolyte. *Phys. Chem. Chem. Phys.* **2013**, *15*, 18600–18606. [[CrossRef](#)] [[PubMed](#)]
30. Porz, L.; Swamy, T.; Sheldon, B.W.; Rettenwander, D.; Frömling, T.; Thaman, H.L.; Berendts, S.; Uecker, R.; Carter, W.C.; Chiang, Y.M. Mechanism of Lithium Metal Penetration through Inorganic Solid Electrolytes. *Adv. Energy Mater.* **2017**, *7*, 1701003. [[CrossRef](#)]
31. Luo, S.; Wang, Z.; Li, X.; Liu, X.; Wang, H.; Ma, W.; Zhang, L.; Zhu, L.; Zhang, X. Growth of lithium-indium dendrites in all-solid-state lithium-based batteries with sulfide electrolytes. *Nat. Commun.* **2021**, *12*, 6968. [[CrossRef](#)]
32. Camacho-Forero, L.E.; Balbuena, P.B. Exploring interfacial stability of solid-state electrolytes at the lithium-metal anode surface. *J. Power Sources* **2018**, *396*, 782–790. [[CrossRef](#)]
33. Wenzel, S.; Weber, D.A.; Leichtweiss, T.; Busche, M.R.; Sann, J.; Janek, J. Interphase formation and degradation of charge transfer kinetics between a lithium metal anode and highly crystalline Li₇P₃S₁₁ solid electrolyte. *Solid State Ion.* **2016**, *286*, 24–33. [[CrossRef](#)]
34. Wenzel, S.; Sedlmaier, S.J.; Dietrich, C.; Zeier, W.G.; Janek, J. Interfacial reactivity and interphase growth of argyrodite solid electrolytes at lithium metal electrodes. *Solid State Ion.* **2018**, *318*, 102–112. [[CrossRef](#)]
35. Hood, Z.D.; Mane, A.U.; Sundar, A.; Tepavcevic, S.; Zapol, P.; Eze, U.D.; Adhikari, S.P.; Lee, E.J.; Sterbinsky, G.E.; Elam, J.W.; et al. Multifunctional Coatings on Sulfide-Based Solid Electrolyte Powders with Enhanced Processability, Stability, and Performance for Solid-State Batteries. *Adv. Mater.* **2023**, *35*, 2300673. [[CrossRef](#)] [[PubMed](#)]
36. Ong, S.P.; Mo, Y.F.; Richards, W.D.; Miara, L.; Lee, H.S.; Ceder, G. Phase stability, electrochemical stability and ionic conductivity of the Li_{10±1}MP₂X₁₂ (M = Ge, Si, Sn, Al or P, and X = O, S or Se) family of superionic conductors. *Energy Environ. Sci.* **2013**, *6*, 148–156. [[CrossRef](#)]
37. Sun, Y.; Suzuki, K.; Hara, K.; Hori, S.; Yano, T.-A.; Hara, M.; Hirayama, M.; Kanno, R. Oxygen substitution effects in Li₁₀GeP₂S₁₂ solid electrolyte. *J. Power Sources* **2016**, *324*, 798–803. [[CrossRef](#)]
38. Suzuki, K.; Sakuma, M.; Hori, S.; Nakazawa, T.; Nagao, M.; Yonemura, M.; Hirayama, M.; Kanno, R. Synthesis, structure, and electrochemical properties of crystalline Li–P–S–O solid electrolytes: Novel lithium-conducting oxysulfides of Li₁₀GeP₂S₁₂ family. *Solid State Ion.* **2016**, *288*, 229–234. [[CrossRef](#)]
39. Murugan, R.; Thangadurai, V.; Weppner, W. Fast Lithium Ion Conduction in Garnet-Type Li₇La₃Zr₂O₁₂. *Angew. Chem. Int. Ed.* **2007**, *46*, 7778–7781. [[CrossRef](#)]
40. Thangadurai, V.; Narayanan, S.; Pinzaru, D. Garnet-type solid-state fast Li ion conductors for Li batteries: Critical review. *Chem. Soc. Rev.* **2014**, *43*, 4714. [[CrossRef](#)]
41. Choi, H.M.; Jun, S.J.; Lee, J.; Ryu, M.-H.; Shin, H.; Jung, K.-N. UV-cured Polymer Solid Electrolyte Reinforced using a Ceramic-Polymer Composite Layer for Stable Solid-State Li Metal Batteries. *J. Electrochem. Sci. Technol.* **2023**, *14*, 85–95. [[CrossRef](#)]
42. Xia, W.H.; Xu, B.Y.; Duan, H.A.; Tang, X.Y.; Guo, Y.P.; Kang, H.M.; Li, H.; Liu, H.Z. Reaction mechanisms of lithium garnet pellets in ambient air: The effect of humidity and CO₂. *J. Am. Chem. Soc.* **2017**, *100*, 2832–2839. [[CrossRef](#)]
43. Sharafi, A.; Yu, S.H.; Naguib, M.; Lee, M.; Ma, C.; Meyer, H.M.; Nanda, J.; Chi, M.F.; Siegel, D.J.; Sakamoto, J. Impact of air exposure and surface chemistry on Li–Li₇La₃Zr₂O₁₂ interfacial resistance. *J. Mater. Chem. A* **2017**, *5*, 13475–13487. [[CrossRef](#)]
44. Cheng, L.; Crumlin, E.J.; Chen, W.; Qiao, R.M.; Hou, H.M.; Lux, S.F.; Zorba, V.; Russo, R.; Kostecki, R.; Liu, Z.; et al. The origin of high electrolyte–electrode interfacial resistances in lithium cells containing garnet type solid electrolytes. *Phys. Chem. Chem. Phys.* **2014**, *16*, 18294–18300. [[CrossRef](#)]
45. Sakuda, A.; Hayashi, A.; Tatsumisago, M. Sulfide Solid Electrolyte with Favorable Mechanical Property for All-Solid-State Lithium Battery. *Sci. Rep.* **2013**, *3*, 2261. [[CrossRef](#)] [[PubMed](#)]
46. Chen, X.Z.; He, W.J.; Ding, L.X.; Wang, S.Q.; Wang, H.H. Enhancing interfacial contact in all solid state batteries with a cathode-supported solid electrolyte membrane framework. *Energy Environ. Sci.* **2019**, *12*, 938–944. [[CrossRef](#)]
47. Shen, X.; Zhang, Q.; Ning, T.; Liu, T.; Luo, Y.; He, X.; Luo, Z.; Lu, A. Critical challenges and progress of solid garnet electrolytes for all-solid-state batteries. *Mater. Today. Chem.* **2020**, *18*, 100368. [[CrossRef](#)]
48. Li, Y.T.; Chen, X.; Dolocan, A.; Cui, Z.M.; Xin, S.; Xue, L.G.; Xu, H.H.; Park, K.; Goodenough, J.B. Garnet Electrolyte with an Ultralow Interfacial Resistance for Li-Metal Batteries. *J. Am. Chem. Soc.* **2018**, *140*, 6448–6455. [[CrossRef](#)]
49. Wu, J.F.; Pu, B.W.; Wang, D.; Shi, S.Q.; Zhao, N.; Guo, X.X.; Guo, X. In Situ Formed Shields Enabling Li₂CO₃-Free Solid Electrolytes: A New Route to Uncover the Intrinsic Lithiophilicity of Garnet Electrolytes for Dendrite-Free Li-Metal Batteries. *ACS Appl. Mater. Interfaces* **2019**, *11*, 898–905. [[CrossRef](#)] [[PubMed](#)]
50. Ruan, Y.; Lu, Y.; Huang, X.; Su, J.; Sun, C.; Jin, J.; Wen, Z. Acid induced conversion towards a robust and lithiophilic interface for Li–Li₇La₃Zr₂O₁₂ solid-state batteries. *J. Mater. Chem. A* **2019**, *7*, 14565–14574. [[CrossRef](#)]
51. Sharafi, A.; Kazyak, E.; Davis, A.L.; Yu, S.; Thompson, T.; Siegel, D.J.; Dasgupta, N.P.; Sakamoto, J. Surface Chemistry Mechanism of Ultra-Low Interfacial Resistance in the Solid-State Electrolyte Li₇La₃Zr₂O₁₂. *Chem. Mater.* **2017**, *29*, 7961–7968. [[CrossRef](#)]

52. Ma, X.; Xu, Y.; Zhang, B.; Xue, X.; Wang, C.; He, S.; Lin, J.; Yang, L. Garnet Si-Li₇La₃Zr₂O₁₂ electrolyte with a durable, low resistance interface layer for all-solid-state lithium metal batteries. *J. Power Sources* **2020**, *453*, 227881. [[CrossRef](#)]
53. Zhou, W.; Zhu, Y.; Grundish, N.; Xin, S.; Wang, S.; You, Y.; Wu, N.; Gao, J.; Cui, Z.; Li, Y. Polymer lithium-garnet interphase for an all-solid-state rechargeable battery. *Nano Energy* **2018**, *53*, 926–931. [[CrossRef](#)]
54. Zhou, W.D.; Wang, S.F.; Li, Y.T.; Xin, S.; Manthiram, A.; Goodenough, J.B. Plating a Dendrite-Free Lithium Anode with a Polymer/Ceramic/Polymer Sandwich Electrolyte. *J. Am. Chem. Soc.* **2016**, *138*, 9385–9388. [[CrossRef](#)] [[PubMed](#)]
55. Han, X.; Gong, Y.; Fu, K.; He, X.; Hitz, G.T.; Dai, J.; Pearse, A.; Liu, B.; Wang, H.; Rubloff, G.; et al. Negating interfacial impedance in garnet-based solid-state Li metal batteries. *Nat. Mater.* **2017**, *16*, 572–579. [[CrossRef](#)] [[PubMed](#)]
56. Wang, C.; Gong, Y.; Liu, B.; Fu, K.; Yao, Y.; Hitz, E.; Li, Y.; Dai, J.; Xu, S.; Luo, W.; et al. Conformal, Nanoscale ZnO Surface Modification of Garnet-Based Solid-State Electrolyte for Lithium Metal Anodes. *Nano Lett.* **2017**, *17*, 565–571. [[CrossRef](#)] [[PubMed](#)]
57. Luo, W.; Gong, Y.; Zhu, Y.; Fu, K.K.; Dai, J.; Lacey, S.D.; Wang, C.; Liu, B.; Han, X.; Mo, Y.; et al. Transition from Superlithiophobicity to Superlithiophilicity of Garnet Solid-State Electrolyte. *J. Am. Chem. Soc.* **2016**, *138*, 12258–12262. [[CrossRef](#)] [[PubMed](#)]
58. Wakasugi, J.; Munakata, H.; Kanamura, K. Effect of Gold Layer on Interface Resistance between Lithium Metal Anode and Li_{6.25}Al_{0.25}La₃Zr₂O₁₂ Solid Electrolyte. *J. Electrochem. Soc.* **2017**, *164*, A1022–A1025. [[CrossRef](#)]
59. Bocharova, V.; Sokolov, A.P. Perspectives for polymer electrolytes: A view from fundamentals of ionic conductivity. *Macromolecules* **2020**, *53*, 4141–4157. [[CrossRef](#)]
60. Meyer, W.H. Polymer electrolytes for lithium-ion batteries. *Adv. Mater.* **1998**, *10*, 439–448. [[CrossRef](#)]
61. Jiang, Y.; Yan, X.; Ma, Z.; Mei, P.; Xiao, W.; You, Q.; Zhang, Y. Development of the PEO based solid polymer electrolytes for all-solid state lithium ion batteries. *Polymers* **2018**, *10*, 1237. [[CrossRef](#)]
62. Chen, R.; Qu, W.; Guo, X.; Li, L.; Wu, F. The pursuit of solid-state electrolytes for lithium batteries: From comprehensive insight to emerging horizons. *Mat. Horiz.* **2016**, *3*, 487–516. [[CrossRef](#)]
63. Sun, X.-G.; Kerr, J.B. Synthesis and characterization of network single ion conductors based on comb-branched polyepoxide ethers and lithium bis (allylmalonate) borate. *Macromolecules* **2006**, *39*, 362–372. [[CrossRef](#)]
64. Irfan, M.; Atif, M.; Yang, Z.; Zhang, W. Recent advances in high performance conducting solid polymer electrolytes for lithium-ion batteries. *J. Power Sources* **2021**, *486*, 229378. [[CrossRef](#)]
65. Ye, L.; Feng, Z. Polymer electrolytes as solid solvents and their applications. In *Polymer electrolytes*; Elsevier: Amsterdam, The Netherlands, 2010; pp. 550–582.
66. Ramesh, S.; Liew, C.-W.; Morris, E.; Durairaj, R. Effect of PVC on ionic conductivity, crystallographic structural, morphological and thermal characterizations in PMMA–PVC blend-based polymer electrolytes. *Thermochim. Acta* **2010**, *511*, 140–146. [[CrossRef](#)]
67. Nicotera, I.; Coppola, L.; Oliviero, C.; Castriota, M.; Cazzanelli, E. Investigation of ionic conduction and mechanical properties of PMMA–PVdF blend-based polymer electrolytes. *Solid State Ion.* **2006**, *177*, 581–588. [[CrossRef](#)]
68. Wheatle, B.K.; Fuentes, E.F.; Lynd, N.A.; Ganesan, V. Design of polymer blend electrolytes through a machine learning approach. *Macromolecules* **2020**, *53*, 9449–9459. [[CrossRef](#)]
69. Przyłuski, J.; Wieczorek, W. Copolymer electrolytes. *Solid State Ion.* **1992**, *53*, 1071–1076. [[CrossRef](#)]
70. Liu, F.; Li, T.; Yang, Y.; Yan, J.; Li, N.; Xue, J.; Huo, H.; Zhou, J.; Li, L. Investigation on the Copolymer Electrolyte of Poly (1, 3-dioxolane-co-formaldehyde). *Macromol. Rapid Commun.* **2020**, *41*, 2000047. [[CrossRef](#)]
71. Chen, Z.; Steinle, D.; Nguyen, H.-D.; Kim, J.-K.; Mayer, A.; Shi, J.; Paillard, E.; Iojoiu, C.; Passerini, S.; Bresser, D. High-energy lithium batteries based on single-ion conducting polymer electrolytes and Li[Ni_{0.8}Co_{0.1}Mn_{0.1}]O₂ cathodes. *Nano Energy* **2020**, *77*, 105129. [[CrossRef](#)]
72. Gao, J.; Wang, C.; Han, D.-W.; Shin, D.-M. Single-ion conducting polymer electrolytes as a key jigsaw piece for next-generation battery applications. *Chem. Sci.* **2021**, *12*, 13248–13272. [[CrossRef](#)] [[PubMed](#)]
73. Porcarelli, L.; Shaplov, A.S.; Bella, F.; Nair, J.R.; Mecerreyes, D.; Gerbaldi, C. Single-ion conducting polymer electrolytes for lithium metal polymer batteries that operate at ambient temperature. *ACS Energy Lett.* **2016**, *1*, 678–682. [[CrossRef](#)]
74. Zhang, H.; Li, C.; Piszcz, M.; Coxa, E.; Rojo, T.; Rodriguez-Martinez, L.M.; Armand, M.; Zhou, Z. Single lithium-ion conducting solid polymer electrolytes: Advances and perspectives. *Chem. Soc. Rev.* **2017**, *46*, 797–815. [[CrossRef](#)] [[PubMed](#)]
75. Rolland, J.; Poggi, E.; Vlad, A.; Gohy, J.-F. Single-ion diblock copolymers for solid-state polymer electrolytes. *Polymer* **2015**, *68*, 344–352. [[CrossRef](#)]
76. Porcarelli, L.; Manojkumar, K.; Sardon, H.; Llorente, O.; Shaplov, A.S.; Vijayakrishna, K.; Gerbaldi, C.; Mecerreyes, D. Single ion conducting polymer electrolytes based on versatile polyurethanes. *Electrochim. Acta* **2017**, *241*, 526–534. [[CrossRef](#)]
77. Zhu, J.; Zhang, Z.; Zhao, S.; Westover, A.S.; Belharouak, I.; Cao, P.F. Single-ion conducting polymer electrolytes for solid-state lithium–metal batteries: Design, performance, and challenges. *Adv. Energy Mater.* **2021**, *11*, 2003836. [[CrossRef](#)]

Disclaimer/Publisher’s Note: The statements, opinions and data contained in all publications are solely those of the individual author(s) and contributor(s) and not of MDPI and/or the editor(s). MDPI and/or the editor(s) disclaim responsibility for any injury to people or property resulting from any ideas, methods, instructions or products referred to in the content.